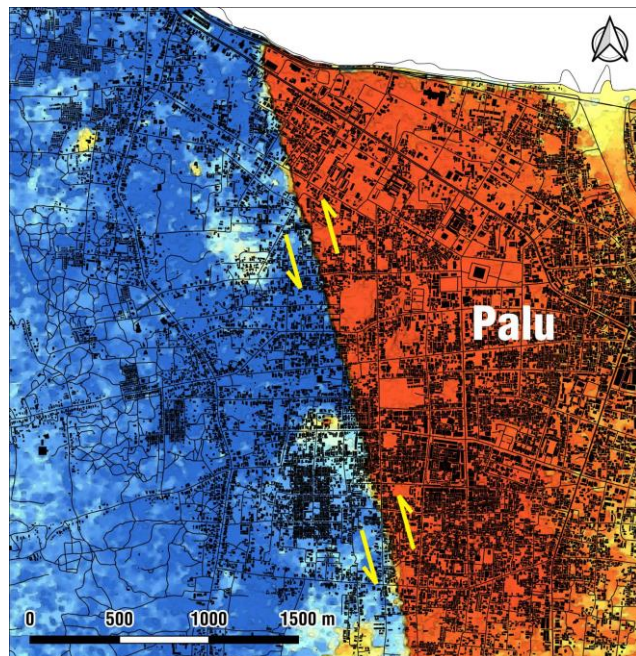


**A preliminary  
report on the M7.5  
Palu earthquake  
co-seismic ruptures  
and landslides  
using image  
correlation  
techniques on  
optical satellite  
data**

19 OCTOBER  
2018

**Sotiris Valkaniotis,  
Athanasios Ganas,  
Varvara Tsironi,  
Aggeliki  
Barberopoulou**



# **A preliminary report on the M7.5 Palu earthquake co-seismic ruptures and landslides using image correlation techniques on optical satellite data<sup>1</sup>**

**Sotiris Valkaniotis<sup>1</sup>, Athanassios Ganas<sup>2</sup>, Varvara Tsironi<sup>2</sup>, Aggeliki Barberopoulou<sup>3</sup>**

<sup>1</sup>*Koronidos Str., Trikala, Greece [valkaniotis@yahoo.com](mailto:valkaniotis@yahoo.com)*

<sup>2</sup>*National Observatory of Athens, Institute of Geodynamics, 11810 Athens, Greece [aganas@noa.gr](mailto:aganas@noa.gr) [barbara.tsir@gmail.com](mailto:barbara.tsir@gmail.com)*

<sup>3</sup>*Stevens Str., Stoneham MA 02180 United States [aggeliki.barberopoulou@gmail.com](mailto:aggeliki.barberopoulou@gmail.com)*

## **Abstract**

We use optical satellite data to map the co-seismic displacements for the Mw=7.5 strike-slip earthquake of 28 September 2018 in Palu, Sulawesi, Indonesia. This was a strike-slip faulting event at shallow depth that occurred within the interior of the Molucca Sea microplate, which is part of the Sunda tectonic plate. Using optical image correlation from Sentinel-2 and Planet imagery, we mapped the surface rupture extent of the earthquake and calculated the co-seismic offsets. Before- and after- the earthquake image acquisitions were analyzed using *MicMac* software and the *MPIC-OPT* service on the ESA Geohazards TEP platform. Our results include the mapping of a) the detailed trace of the ruptured fault at the southern part of the region (Palu segment) and b) a more complex deformation pattern at the northern part of the rupture. Analysis of the horizontal displacement field and sequential profiles across the fault also enabled mapping of the fault zone complexity, secondary faulting, fault zone width and large co-seismic gravitational phenomena. A mean displacement of 3-5 metres was calculated for a total earthquake rupture length of more than 140 km. Our results agree with the focal mechanism solution for the earthquake which indicates that the rupture occurred on a left-lateral, north-south striking fault. The significance of this event is also associated with the severity of the tsunami impact attributed to a strike slip fault. Further investigation is necessary to determine the source of the tsunami as primarily tectonic or due to another mechanism although a more complex mechanism is likely.

---

<sup>1</sup> Report submitted to EMSC on 19 October 2018 12:00 UTC

## 1. Introduction

A moment magnitude 7.5 earthquake struck north of Palu, Indonesia on September 28, 2018 at 6:03 pm local time (10:03 am UTC). The earthquake caused severe damage to buildings and infrastructure and is responsible for two thousand dead and many more injured (numbers are likely to increase). The impact of this event is attributed to ground shaking, major liquefaction, landslides and a tsunami. The Indonesian archipelago is known for its catastrophic earthquakes and tsunamis as well as the occurrence of landslide induced tsunamis. This was a large, strike-slip faulting event at shallow depth that occurred within the interior of the Molucca Sea microplate, which is part of the Sunda tectonic plate.

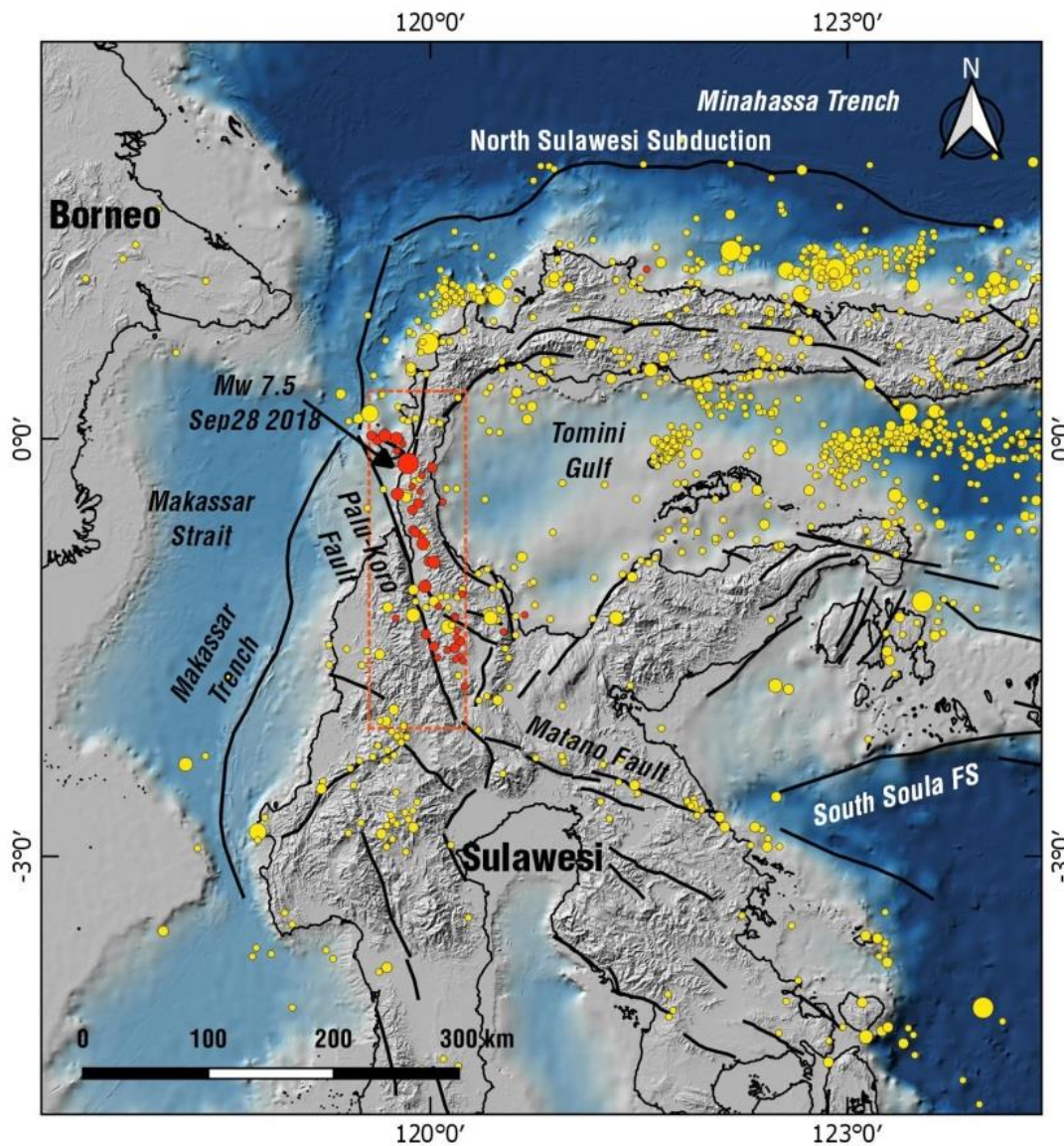


**Figure 1.** Tectonic setting and seismicity of Sulawesi island, Indonesia. Major active tectonic structures and faults are shown. Red dotted box marks the Palu-Koro fault zone, associated with the M7.5 September 2018 earthquake ruptures. Yellow solid circles are instrumental M>5 seismicity from IRIS (1970-2018), and red solid circles are epicentres from the M7.5 earthquake sequence (with M>4).

Sulawesi Island (Fig. 1) is located in the triple junction of the Australian, Philippine and Sunda plates (the Sunda plate is the eastern part of Eurasia). The Australian and Philippine plates subduct beneath the Sunda plate with a rate of 75 and 90 mm/yr, respectively. To the south of Sulawesi, the E-W trending plate boundary zone which extends from eastern Indonesia to the New Guinea Trench accommodates the relative motion between Australian and Pacific plates by transpressive faulting and block rotations (Tregoning et al., 2000; Wallace et al., 2004). The subduction of the Australian plate beneath the Sunda plate is taking place at the Sunda-Banda Arc where it transitions to the Java trench. The Java Trench evolves into the collision with Australia about 600 km to the south of Sulawesi. So, the Sulawesi Island accommodates the convergence of the continental fragments with the active trench of Sunda and it is an example of how the collision occurs without mountain building but with the rotation of crustal blocks (Socquet et al., 2006). There is a 42 mm/yr of relative block motion that is accommodated on the Palu-Koro left-lateral strike-slip fault zone (see red box in Fig. 1; Socquet et al., 2006).

In this report we use the method of optical image correlation to map the surface rupture extent of the earthquake and calculate co-seismic offsets. The shallowness of the source and the magnitude of the event enabled the excellent opportunity to use remote sensing to map the ruptures and associated secondary effects (landslides etc.). Our remote sensing data comprised Sentinel-2 (10-m resolution) and Planet optical imagery (3-m resolution) before and after the earthquake. The image acquisitions were analyzed using *MicMac* software and the *MPIC-OPT* service on ESA's Geohazards TEP. The *MPIC-OPT* is a Multiple-Pairwise Image Correlation technique which targets the detection and measurement of horizontal ground motion based on sub-pixel image correlation. Our results include the extraordinary mapping of: a) the detailed trace of the ruptured fault at the southern part of the region (Palu segment) and b) a more complex deformation pattern at the northern part of the rupture. Our results agree with the focal mechanism solution for the earthquake which indicates that the rupture occurred on a left-lateral, north-south striking fault. In addition, we analyze the horizontal displacement field and construct sequential profiles across the fault in order to map displacement distribution, secondary faulting, fault zone width and large co-seismic gravitational phenomena. The significance of this event is also associated with the severity of the tsunami impact attributed to a strike slip fault.

## **2. Characteristics of the seismic event**

The 28 September 2018, M 7.5 earthquake on Sulawesi, Indonesia occurred as a result of strike-slip faulting at shallow depths within the interior of the Molucca Sea microplate, part of the broader Sunda tectonic plate. The focal mechanism solutions for the earthquake (Fig. 2) indicate that the rupture occurred on either a left-lateral (north-south) striking fault, or along a right-lateral (east-west) striking fault. At the location of



### 3. Measuring co-seismic deformation from optical image correlation

We used optical satellite acquisitions after the earthquake in order to measure horizontal displacement from the fault rupture. Sub-pixel correlation method (Scambos et al., 1992; Van Puymbroeck, 2000; Leprince et al., 2007) applied on two images acquired at different times and ortho-rectified, enables detection of homologous points by correlation methods with a theoretical sensitivity of  $1/10^{\text{th}}$  of a pixel. Shift between corresponding points on the two images relates to the displacement that occurred between the acquisition of the two images.

Sub-pixel correlation applied to high-resolution satellite images has shown the efficiency of this technique for measuring ground displacements due to earthquakes (Klinger et al., 2006; Barisin et al., 2009; Rosu et al., 2014). A 2-D displacement field with two components, E-W and N-S is produced that can be analysed and interpreted in order to identify and measure horizontal displacements.

For this analysis, we used the *MicMac* open-source photogrammetry software, and *MPIC-OPT* (Multiple Pairwise Image Correlation of OPTical image Time-series – Stumpf et al., 2017) service on Geohazards TEP. Optical imagery available for this analysis was Sentinel-2 (10 m resolution) from Copernicus/ESA covering the full region, and Planet (3 m resolution) from Planet Labs (Planet 2018) for a 20 km part of the fault near Palu. Post-earthquake acquisitions of Sentinel-2 were made on October 2, 2018 and for Planet images on October 1<sup>st</sup>, 2018, respectively. Preliminary results from MPIC-OPT processing of Sentinel-2 frames are shown at Figure 3.

Although large parts of the area around the fault rupture are missing due to cloud cover or correlation failure, there is a clear delineation of the fault rupture at the central/southern part, while northern part is poorly defined as a result of cloud cover and poor coherence.

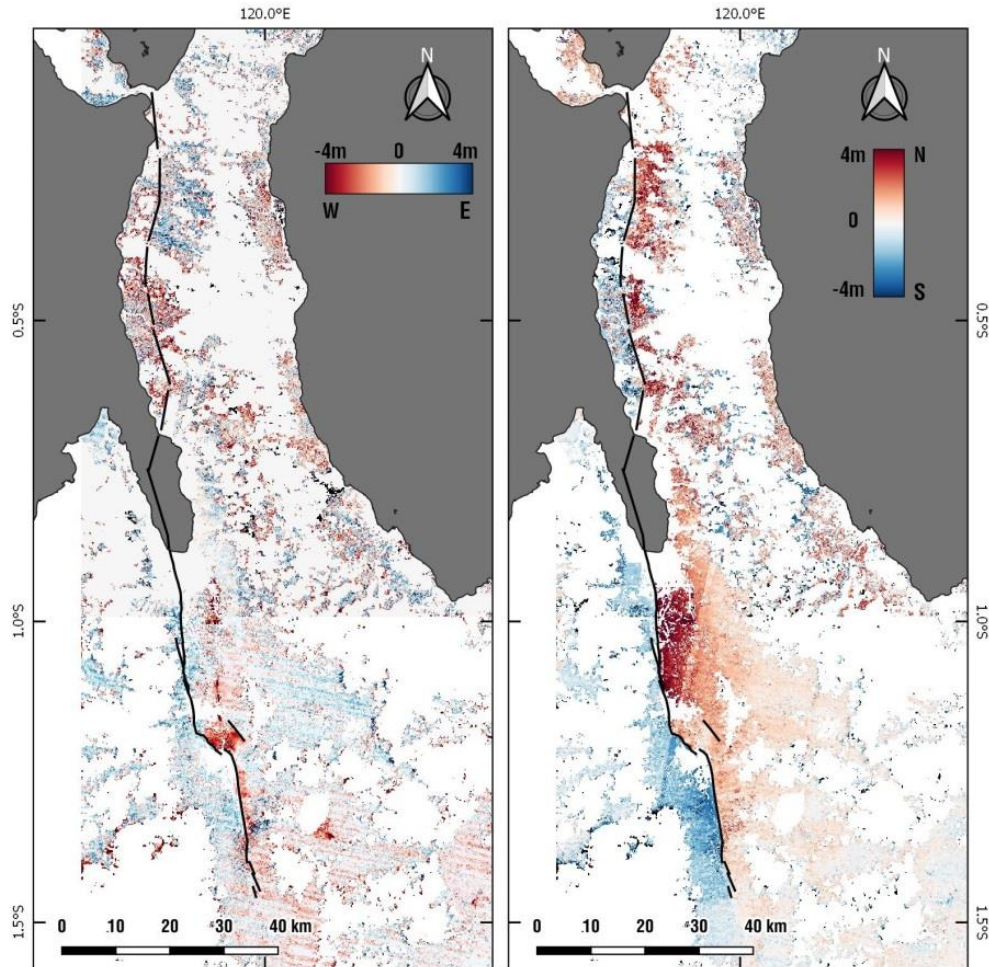


**Figure 3.** Horizontal displacement of several metres along the M7.5 Palu, Sulawesi earthquake rupture produced from Sentinel-2 optical imagery using the MPIC-OPT service. Left-lateral movement of the fault is apparent from the N-S component (right panel: red is towards north, blue towards south). E-W component (left panel) is more indicative of large gravitational coseismic features. Total fault rupture exceeded 140 km in length.

Using the MicMac software (Rosu et al. 2014; Rupnik et al. 2017), we also obtained a satisfactory imaging of the earthquake displacement field from Sentinel-2 images (Figure 4). The fault rupture trace is identified by the merging of opposing displacement gradients. The dominant component of the fault is N-S (left-lateral slip) while the E-W component mainly marks locations of large surface displacements (landslides, lateral spreading). Based on optical correlation results, we mapped a > 140 km rupture length for the M7.5 earthquake. Fault slip is mainly strike-slip (left-lateral) with a small reverse component. Fault rupture probably involves multiple segments and a large part of the Palu-Koro fault. At least two major steps are involved, transferring the strike-slip rupture through different segments and faults. The best documented left-step connects Palu segment with the southernmost fault segment (Fig. 4), where a normal (?) NW-SE fault at the eastern side of the valley was probably activated by the earthquake as it is inferred by the E-W displacement field.

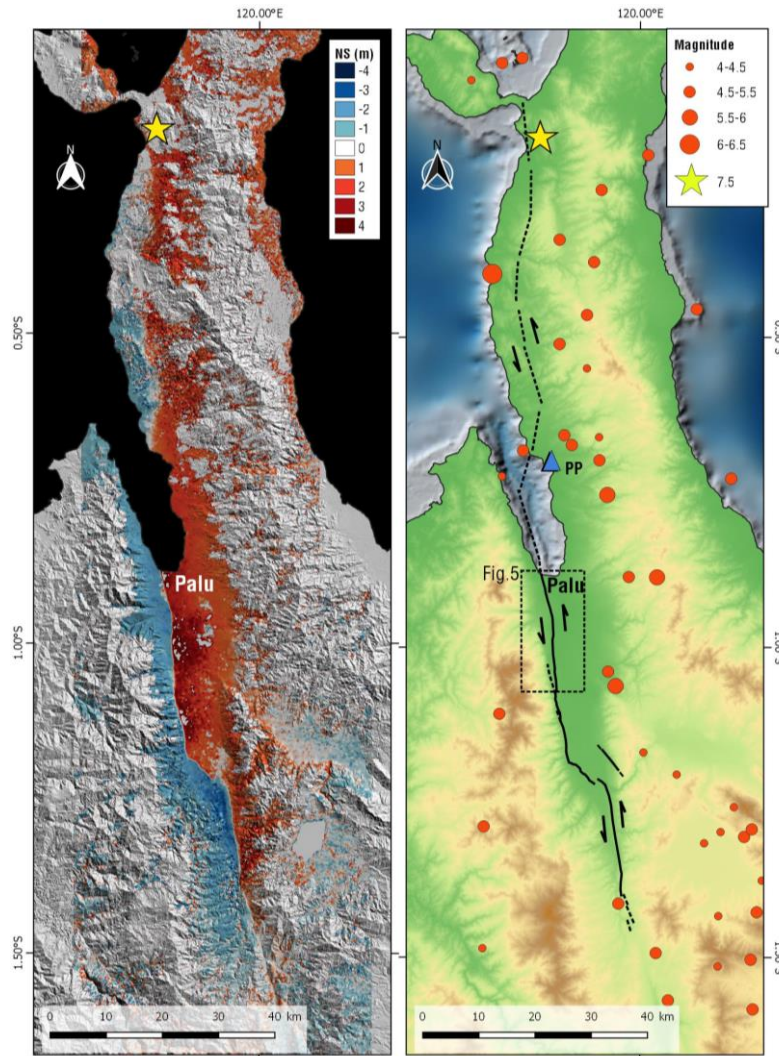


**Figure 4.** Left panel): Horizontal displacement (N-S component) using optical image correlation from Sentinel-2 imagery, processed with MicMac software. Areas in red color moved to the north; areas in blue moved towards the south. The horizontal displacement is larger than 4 m along a large portion of the rupture. Right panel) delineation of the rupture trace (thick black lines), with dotted lines depicting areas showing lack of data or low-quality data. The Pantoloan Port tide gauge position is marked with a blue triangle. Red solid circles indicate USGS epicentres ( $M > 4$ ) for the period Sep 28 – Oct 12, 2018.

Planet images with a high ground resolution of 3 m were used to map the fault rupture zone in more detail (Figure 5). Because of improved resolution over Sentinel-2, it enabled a finer detail of both the fault horizontal deformation and its trace/structure. Preliminary results for a 20 km section of the fault crossing the Palu alluvial valley, revealed a rather clear and simple rupture that can be followed along the western part of the valley. A post-earthquake field report by PVMBG-CVGHM (*Pusat Vulkanologi dan Mitigasi Bencana Geologi*) included fault offset measurements so as this allowed us to validate our image processing results. Using a profile across the reported site, we measured **5.4 m** of fault offset from the Planet displacement data, which is a good match with respect to the **4.6 - 5.8 m** offset measured by PVMBG-CVGHM geologists (Figure 6). The maximum displacement (horizontal) was mapped at the centre-south

part, along Palu fault segment. Our results indicate that the rupture started near the epicentre (Fig. 4) where it was accommodated along a poorly-defined fault zone at an approximate N-S orientation, then was transferred towards the south along the Palu-Koro fault, up to the southernmost end.

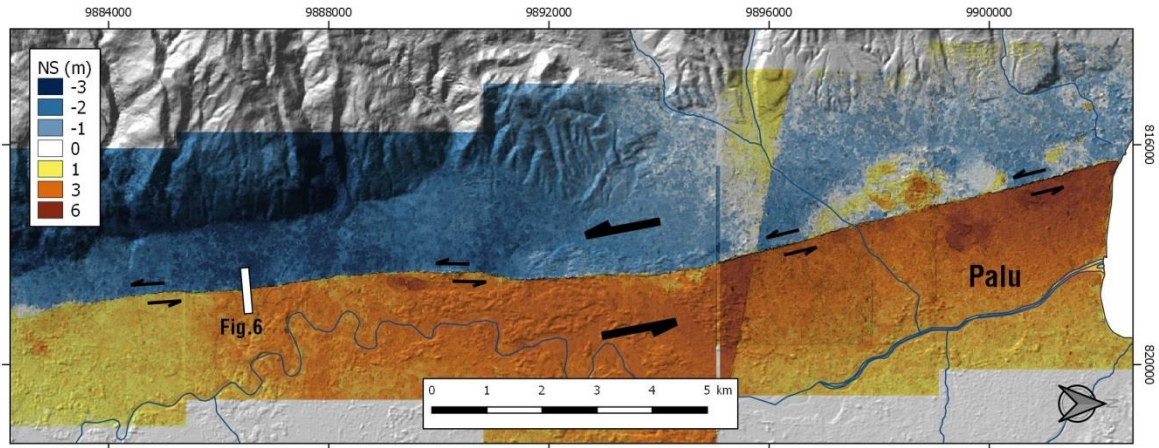


**Figure 5.** Detailed map of the co-seismic displacement trace of the Palu fault segment, obtained by image correlation using MicMac software and Planet imagery (see map location in Figure 4). Surface ruptures along the Palu segment show little complexity and a single rupture plane. Shaded relief is from DEMNAS 8m digital elevation model (tides.big.go.id/DEMNAS). Location of Figure 6 is outlined with a white rectangle.

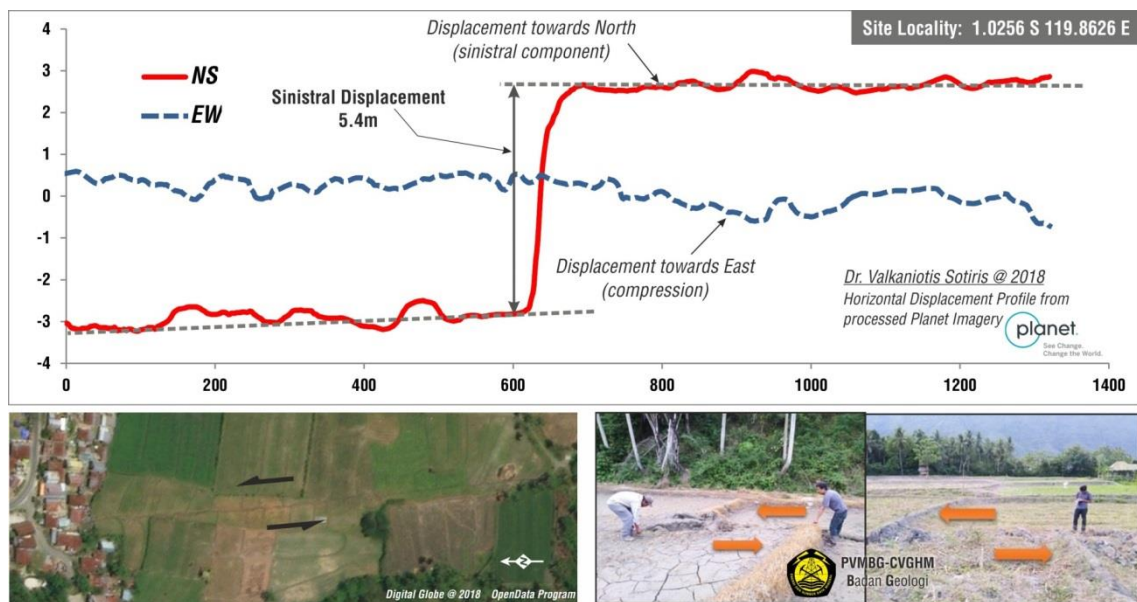


**Figure 6.** Comparison of displacement extracted from Planet imagery for Palu fault co-seismic rupture, with field data reported from PVMBG-CVGHM at the same locality [https://twitter.com/vulkanologi\\_mbg/status/1050396131216175105](https://twitter.com/vulkanologi_mbg/status/1050396131216175105). Field measurements range from 4.6 - 5.8 m and validate the 5.4 m left-lateral offset measured from optical correlation. The data comprise a E-W 50 m wide swath profile. Site location is indicated in Figure 5.

### 3. Co-seismic landslides and gravitational phenomena

The September 28, 2018 earthquake was responsible for the generation of multiple landslides around the coastal area that was affected by strong ground motions. The majority of human losses in Palu region are attributed to km-size, massive slides at the alluvial valley sediments (Figure 7). One of the major slides mobilized hundreds of buildings inside the western part of Palu city. However, most of the large slides on the Palu valley are found in the eastern part, located along a broad zone of surface displacement (Fig. 7 & 8). Multiple landslides were also identified at the mountainous and hilly areas, on either side of the main fault rupture. The large areas that show significant horizontal displacement of tens of metres, were also identified on the optical imagery. These unstable zones, as it is indicated by topography, correlate with the fan piedmont line, where the coarse-sediment alluvial fans terminate and the fine-sediment alluvial floodplain develops. Our preliminary interpretation involves a permanent displacement of the unconsolidated alluvial sediments that was triggered by the strong ground motion, and a possible liquefaction of sediment layers below the surface.

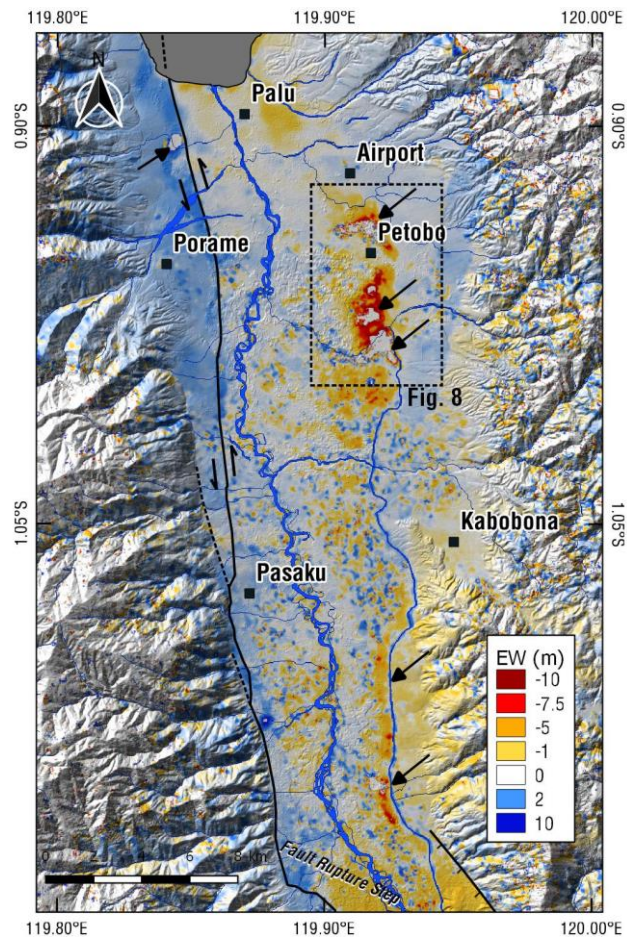


**Figure 7.** Surface deformation associated with coseismic gravitational effects displayed as E-W horizontal displacement. Red-yellow colors mark the main zone of deformation at the eastern side of Palu alluvial valley, that was dislocated towards west. Arrows mark the location of major catastrophic slides. Dotted box marks the location of Fig. 8.

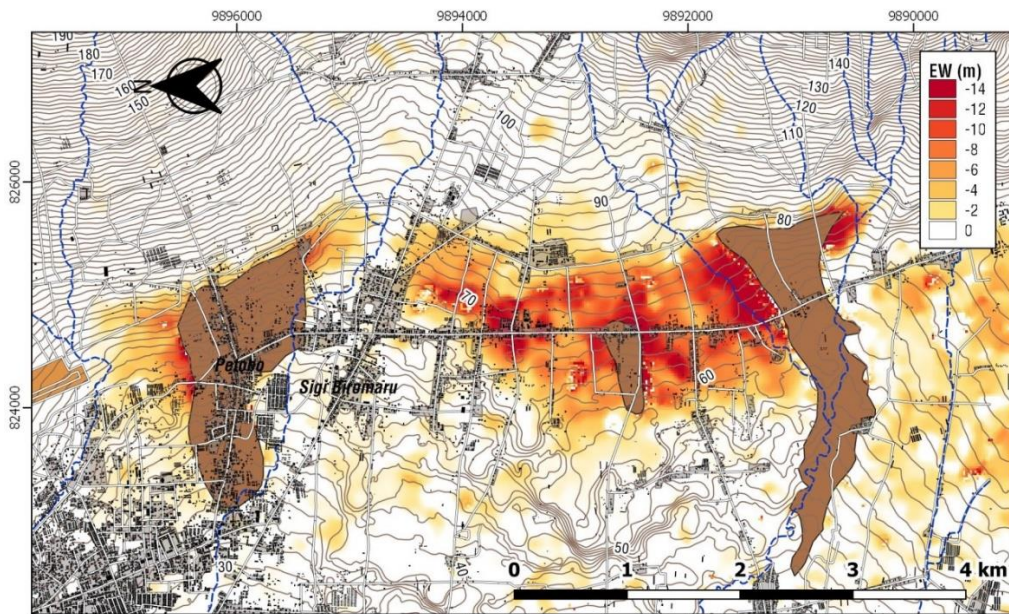


**Figure 8.** Extensive ground displacement on the eastern Palu valley. Brown polygons are large catastrophic slides that caused major loss of life and swept small settlements (see Figure 7 for location). Red and yellow color indicates the horizontal displacement (movement towards west), reaching locally 14 m. There is a wide zone of 1-2 km width that was dislocated towards west.

#### 4. Tsunami – what we know so far

The September 28, 2018 earthquake and tsunami that hit central Sulawesi in Indonesia is of particular interest and significance. A M7.5 earthquake on a strike slip fault caused a catastrophic tsunami. Although strike-slip faults have been previously associated with tsunamis (e.g. Barberopoulou et al. 2011) most tsunami studies tend to exclude such fault types. Strike slip faults are also challenging for tsunami warning systems as they are generally considered non-tsunamigenic.

The earthquake epicenter was approximately 80 km north of Palu City, one of the hardest hit locations from this earthquake, landslides, liquefaction and tsunami. Palu city is at the end of a narrow, elongated harbor that may also have contributed to the pattern of damage from the tsunami as evidenced in the field surveys and eyewitness observations collected so far. More specifically, one of the first international teams (Muhari et al., 2018) to visit the impacted areas on September 28, 2018, surveyed areas of the south and east coast of the bay of Palu including Palu city, Mamboro and Pantoloan. The largest inundation heights<sup>2</sup> were found on the east side of the bay of Palu in Mamboro (7.3 m) and in Pantoloan (4.9 m) while a measurement of 10.1 m inundation height in Mamboro is considered an outlier, probably a localized effect and not indicative of the general tsunami effects in the area. Eyewitness observations from the same survey support such large localized values but indicate a larger value of the

<sup>2</sup> Inundation height is defined as the tsunami wave height measured with respect to still water level

order of 11 m. Similar outliers have been found in tsunami field surveys before, such as in the post-tsunami disaster environment in Chile after the Feb 27, 2010 Chile tsunami (Annunziato et al., 2010). Inundation depths<sup>3</sup> of 4.5 m and 4.8 m were also recorded in Mamboro. The nearest tide gauge record from Pantoloan (Fig. 9) shows wave heights in excess of 1.5 m (0-peak) and a water elevation change of 3.8 m (peak-trough).

Based on the work presented here, in addition to early tsunami field survey results and modeling there may be several factors that have intensified tsunami waves generated by this earthquake. Co-seismic landslides seen in satellite imagery on the E-W direction (Fig. 7) suggest the possibility of landslide induced waves inside Palu bay. Since a tectonic tsunami partially explains observations, landslide generated waves may explain the large waves observed within the bay and the short time for residents to respond. Other contributing factors likely are the narrow bay and reflections of waves across the width of the bay. A quick observation of the tide gauge (raw data is not available to the authors at this time) shows oscillations on the order of few mins following the large first arrival which may be due to sloshing produced as waves reflect off the sides of the bay on the E-W direction.

As of October 15, 2018 the ASEAN Coordinating Centre for Humanitarian Assistance (AHA Centre; <http://ahacentre.org>) reports the death toll at a total of 2100 fatalities in addition to approximately 700 missing. Although, the damage extent and life loss is a result of a combination of the direct effects of the earthquake (e.g. ground shaking) and earthquake effects such as liquefaction and landslides, the catastrophic tsunami likely attributed largely to the death toll. Based on eyewitness observations and tide gauge data available it is believed that there were only few minutes for people to evacuate coastlines in the Palu bay before the first waves arrived. The cancellation of the tsunami warning issued may have not been therefore a critical factor in the life loss.

However, the challenges associated with strike slip fault rupturing and tsunami warning systems for faults at near and regional distances will have to be investigated further. Information from field survey teams responding to a request from Indonesia, UNESCO's Intergovernmental Oceanographic Commission, in collaboration with Indonesian authorities in addition to research on the specific peculiarities of this event, will provide useful information to this end.

---

<sup>3</sup> Inundation depth is defined as the depth of water with respect to topography

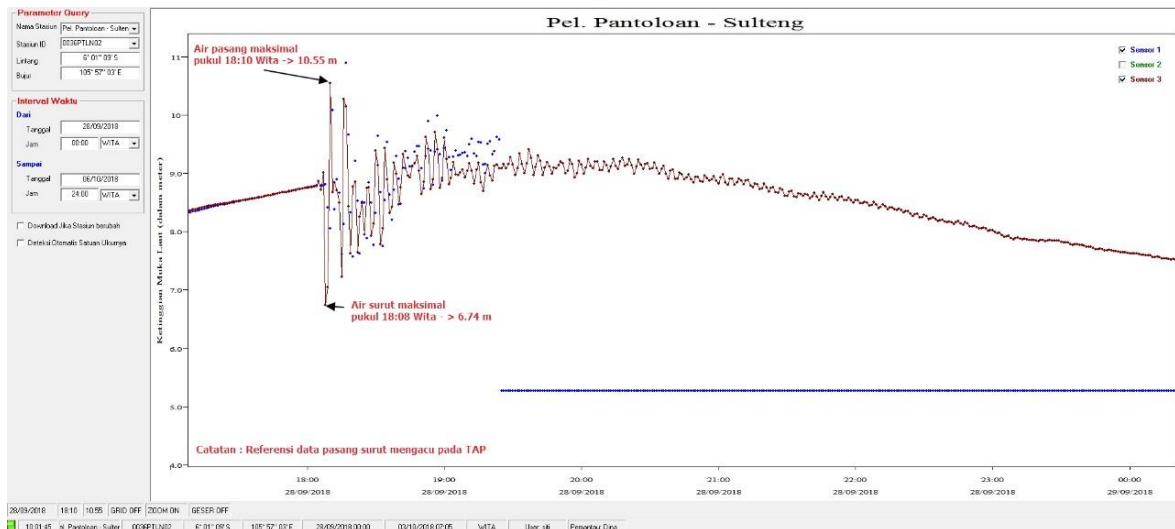


**Figure 9.** Pantoloan Port tide gauge of BMKG (Badan Meteorologi, Klimatologi, dan Geofisika) showing a record of the September 28, 2018 Palu, Sulawesi tsunami. Arrows show largest peak and trough indicating the 3.8 water elevation change recorded. The Pantoloan tide gauge is the nearest water level record available to Palu, and the only one from Palu bay. Tide gauge location is marked in Figure 4.

## 5. Acknowledgements

We thank Copernicus/ESA for providing free-access to Sentinel-2 data and Planet Labs Inc. for providing Planet optical imagery (© 2018 Planet Labs). MicMac is an open-source photogrammetry software developed by IGN/ENSG (<https://github.com/micmacIGN/micmac>). Access to pre-operational Geohazards Exploitation Platform ([geohazards-tep.eo.esa.int](http://geohazards-tep.eo.esa.int)) was granted under the Early Adopters Programme (Corinth Rift Laboratory). Topographic and basemap data were made available from the Center for Geospatial Information Management and Dissemination of Geospatial Information Agency (BIG), Indonesia.

We would like to thank Jason R. Patton, Yan Klinger, Eric Fielding, Michael Foumelis, Marcello de Michele, Dave Petley, Ken Hudnut, Austin Elliot, Anthony Lomax, Joe Mascaro, Pamumpuni Astyka, Lucile Bruhat, Baptiste Gombert, Pablo Ampuero, Stephane Baize, Robin Lacassin, Jamie Gurney, Stacey Martin, Bas Altena and others, for discussion, comments and input.

## 6. References

Annunziato, A., Franchello, G., Barberopoulou, A., 2010. 27 February 2010 Chile tsunami post-event survey mission. European Commission Joint Research Centre Scientific and Technical Reports, 58576. 268 pp <http://publications.jrc.ec.europa.eu/repository/handle/JRC58576>

Barberopoulou, A., Legg, M.R., Uslu, B., Synolakis, C.E., 2011. Reassessing the tsunami risk in major ports and harbors of California I: San Diego. *Natural Hazards* 58, 479–496. doi:10.1007/s11069-010-9681-8

Barisin, I.; Leprince, S.; Parsons, B.; Wright, T. 2009. Surface displacements in the September 2005 Afar rifting event from satellite image matching: Asymmetric uplift and faulting. *Geophys. Res. Lett.*, 36, L07301

Geohazards Exploitation Platform and Portal <https://geohazards-tep.eo.esa.int>

Klinger, Y., Michel, R., King, G.C.P., 2006. Evidence for an earthquake barrier model from Mw 7.8 Kokoxili (Tibet) earthquake slip-distribution. *Earth Planet. Sci. Lett.*, 242, 354–364.

Leprince, S., Barbot, S., Ayoub, F., Avouac, J.-P., 2007. Automatic and precise orthorectification, coregistration, and subpixel correlation of satellite images, application to ground deformation measurements. *IEEE Trans. Geosci. Remote Sens.* 45 (6), 1529–1558. <http://dx.doi.org/10.1109/TGRS.2006.888937>

Muhari, A. et al. 2018. Finding of the unexpected tsunami due to the strike-slip fault at central Sulawesi, Indonesia on 28 September 2018, from the preliminary field survey at Palu [http://irides.tohoku.ac.jp/media/files/earthquake/eq/2018\\_sulawesi\\_eq/IRIDeS\\_report\\_Palu\\_survey\\_20181015.pdf](http://irides.tohoku.ac.jp/media/files/earthquake/eq/2018_sulawesi_eq/IRIDeS_report_Palu_survey_20181015.pdf)

Planet Team, 2018. Planet Application Program Interface: In Space for Life on Earth. San Francisco, CA. <https://api.planet.com>

Rosu, A.-M., Pierrot-Deseilligny, M., Delorme, A., Binet, R., Klinger, Y., 2014. Measurement of ground displacement from optical satellite image correlation using the free open-source software MicMac. *ISPRS Journal of Photogrammetry and Remote Sensing*, 100, 48-59 <https://doi.org/10.1016/j.isprsjprs.2014.03.002>

Rupnik, E., Daakir, M., Pierrot-Deseilligny, M., 2017. MicMac – a free, open-source solution for photogrammetry. *Open Geospatial Data, Software and Standards*, 2(14) <https://doi.org/10.1186/s40965-017-0027-2>

Sentinel-2 maps for the 2018 Palu Indonesian earthquake [http://www.esa.int/Our\\_Activities/Observing\\_the\\_Earth/Copernicus/Sentinel-2/Sentinel-2\\_maps\\_Indonesia\\_earthquake](http://www.esa.int/Our_Activities/Observing_the_Earth/Copernicus/Sentinel-2/Sentinel-2_maps_Indonesia_earthquake)

Scambos, T.A., Dutkiewicz, M.J., Wilson, J.C., Bindschadler, R.A., 1992. Application of image cross-correlation to the measurement of glacier velocity using satellite image data. *Remote Sens. Environ.*, 42, 177–186.

Socquet, A., W. Simons, C. Vigny, R. McCaffrey, C. Subarya, D. Sarsito, B. Ambrosius, and W. Spakman, 2006. Microblock rotations and fault coupling in SE Asia

triple junction (Sulawesi, Indonesia) from GPS and earthquake slip vector data, *J. Geophys. Res.*, 111, B08409, doi: 10.1029/2005JB003963

Stumpf, A., Malet, J.P. and Delacourt, C., 2017. Correlation of satellite image time-series for the detection and monitoring of slow-moving landslides. *Remote Sensing of Environment*, 189, 40-55 <https://doi.org/10.1016/j.rse.2016.11.007>

The AHA Centre Home of One ASEAN One Response <https://ahacentre.org/>

Tregoning, P., McQueen, H., Lambeck, K., Jackson, R., Little, R., Saunders, S., & Rosa, R. 2000. Present-day crustal motion in Papua New Guinea. *Earth, Planets and Space*, 52 (10), 727-730.

Van Puymbroeck, N., Michel, R., Binet, R., Avouac, J.-P., & Taboury, J., 2000. Measuring earthquakes from optical satellite images. *Applied Optics*, 39(20), 3486. <https://doi.org/10.1364/ao.39.003486>

Wallace, L. M., C. Stevens, E. Silver, R. McCaffrey, W. Loratung, S. Hasiata, R. Stanaway, R. Curley, R. Rosa, and J. Taugaloidi, 2004. GPS and seismological constraints on active tectonics and arc-continent collision in Papua New Guinea: Implications for mechanics of microplate rotations in a plate boundary zone, *J. Geophys. Res.*, 109, B05404, doi: 10.1029/2003JB002481

Web sites (last accessed 17/10/2018)

<https://www.emsc-csem.org/Earthquake/earthquake.php?id=715248>

<https://earthquake.usgs.gov/earthquakes/eventpage/us1000h3p4/executive>

<https://geofon.gfz-potsdam.de/eqinfo/event.php?id=gfz2018tabt>

<https://www.emsc-csem.org/Earthquake/tensors.php?view=4>